

Supporting Information for

Flexible and bright surface-enhanced electrochemiluminescence film constructed from efficient aggregation-induced emission luminogens for biomolecules sensing

Zihua Li,^{*,a} Yusheng Zhou,^a Yuhan Cui^a and Guodong Liang^{*,a}

^a*PCFM Lab, School of Materials Science and Engineering, Sun Yat-Sen University, Guangzhou, 510275, China.*

* Corresponding authors: Dr. Zihua Li and Prof. Guodong Liang

E-mail address: lizh259@mail2.sysu.edu.cn; lgdong@mail.sysu.edu.cn

Supplementary figures

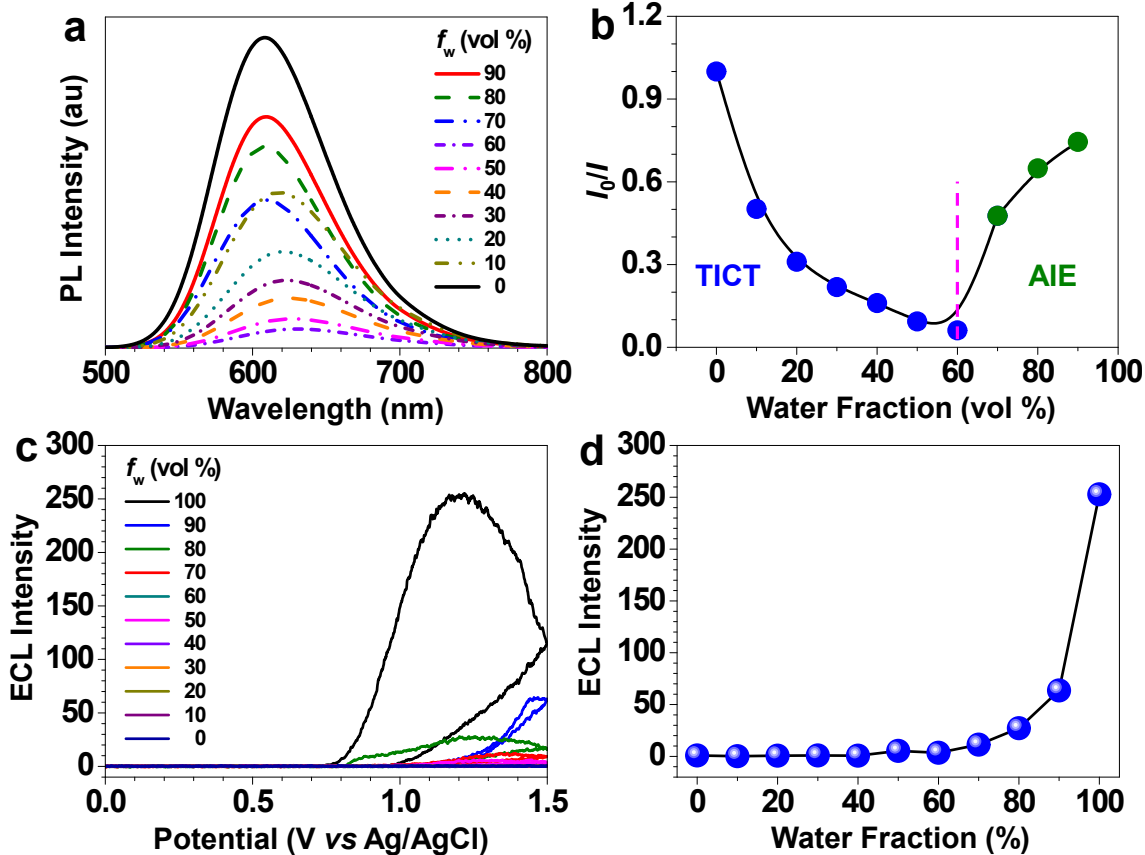


Figure S1. (a) Fluorescence spectra and (b) the plot of the relative fluorescence intensity (I/I_0) of AIEgen in THF/H₂O mixed solvents. I_0 : emission intensity in pure THF. Excitation: 460 nm. (c) ECL-potential profiles of the AIEgen film on GCE in THF/H₂O mixed solvents. (d) Plot of ECL intensity against water fraction.

It is noted that PL intensity of the AIEgen (BTD-TPA) is strongest in pure THF (Figure S1a,b), while ECL signal is not detected in pure THF solutions using glassy carbon (Figure S1c,d). PL spectra of the AIEgen/THF solution are excited by UV light. Most of AIEgen molecules are excited and involved in light emission, leading to strong PL intensity. In contrast, ECL of AIEgen/THF solution is triggered by electrochemical reactions near the electrode surface. AIEgen concentration near electrode surface is low in the AIEgen/THF solution, leading to low concentration of excited AIEgen molecules and faint ECL.

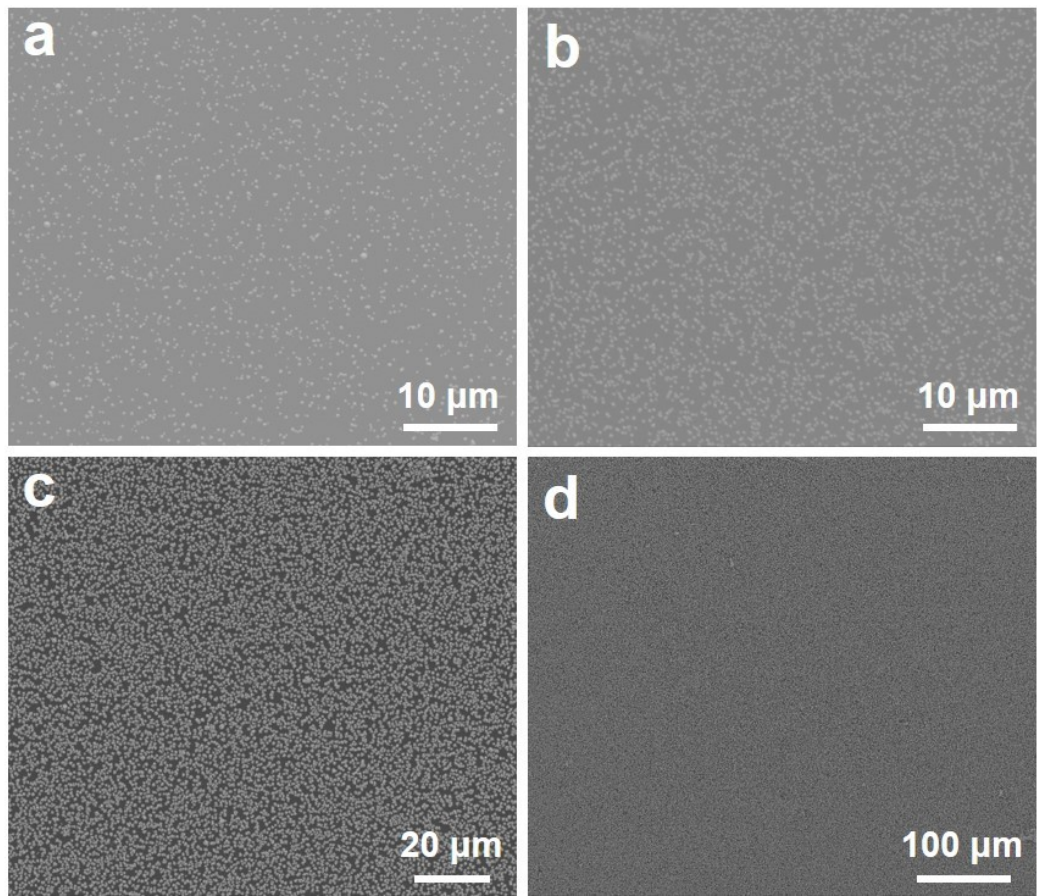


Figure S2. Low-magnification SEM images of AuNPs electrochemically deposited on GCE at different deposited cycles. (a) 1 cycle, (b) 20 cycles, (c) 50 cycles, and (d) 100 cycles.

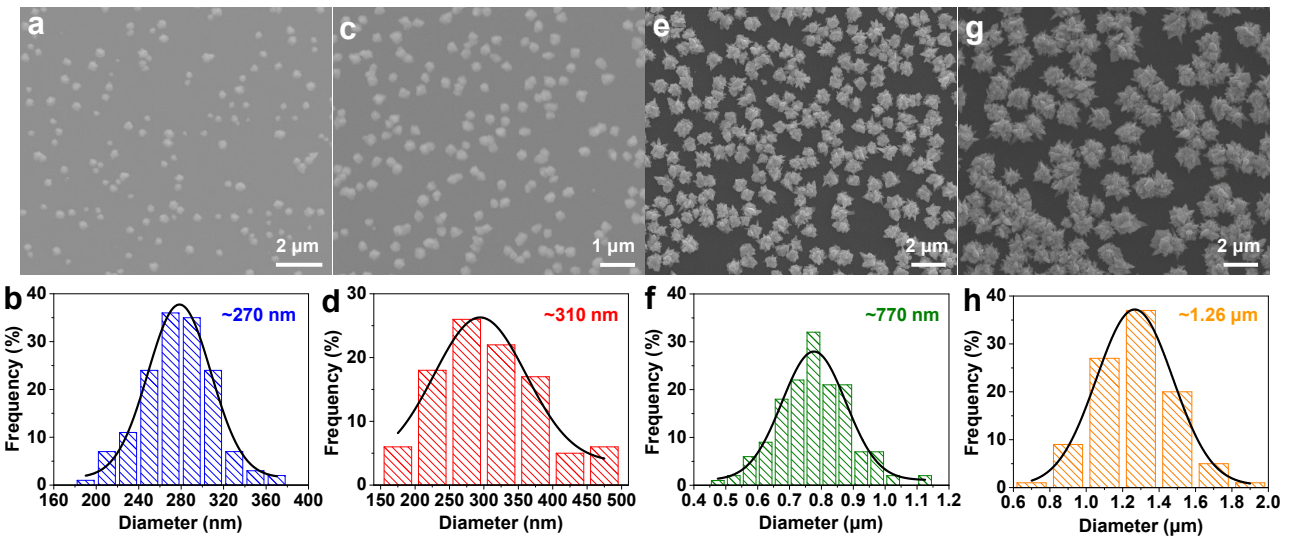


Figure S3. High-magnification SEM images and diameter distribution of AuNPs electrochemically deposited on GCE at different deposited cycles. (a) and (b) 1 cycle, (c) and (d) 20 cycles, (e) and (f) 50 cycles, (g) and (h) 100 cycles.

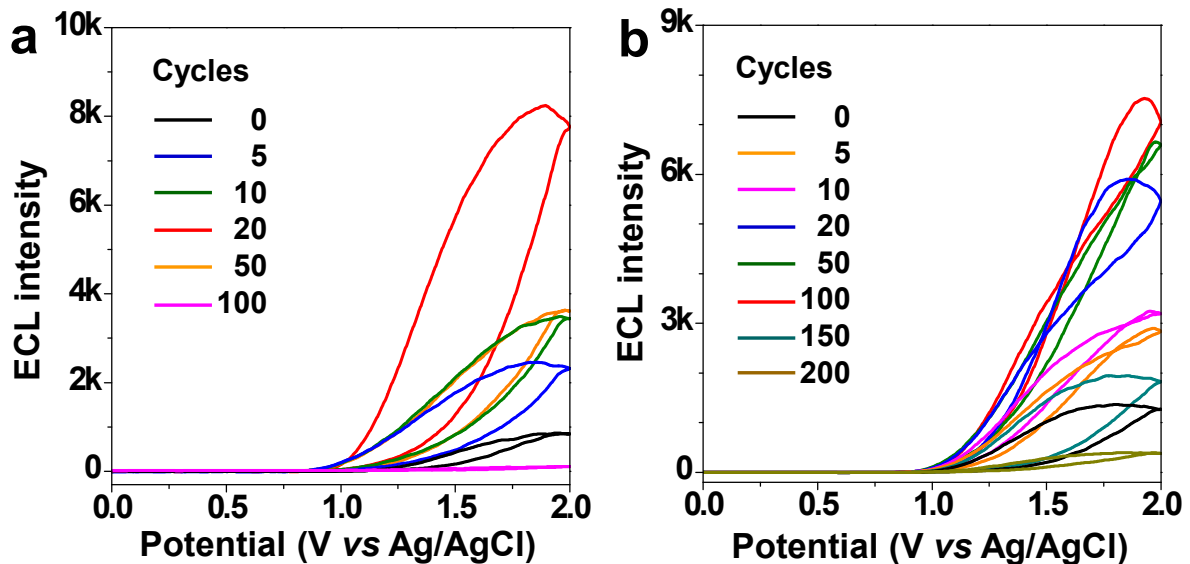


Figure S4. ECL-potential profiles of the AIEgen film on (a) GCFC, and (b) GCFP at different electrodeposition cycles in 0.2 M of PBS solution containing 300 mM of TEOA, pH = 8.

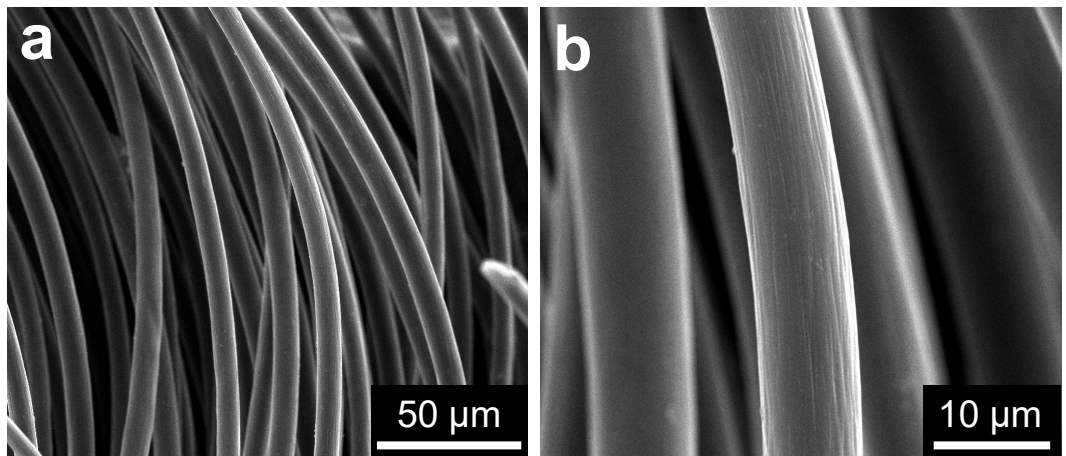


Figure S5. (a) Low-magnification and (b) high-magnification SEM images of bare CFC.

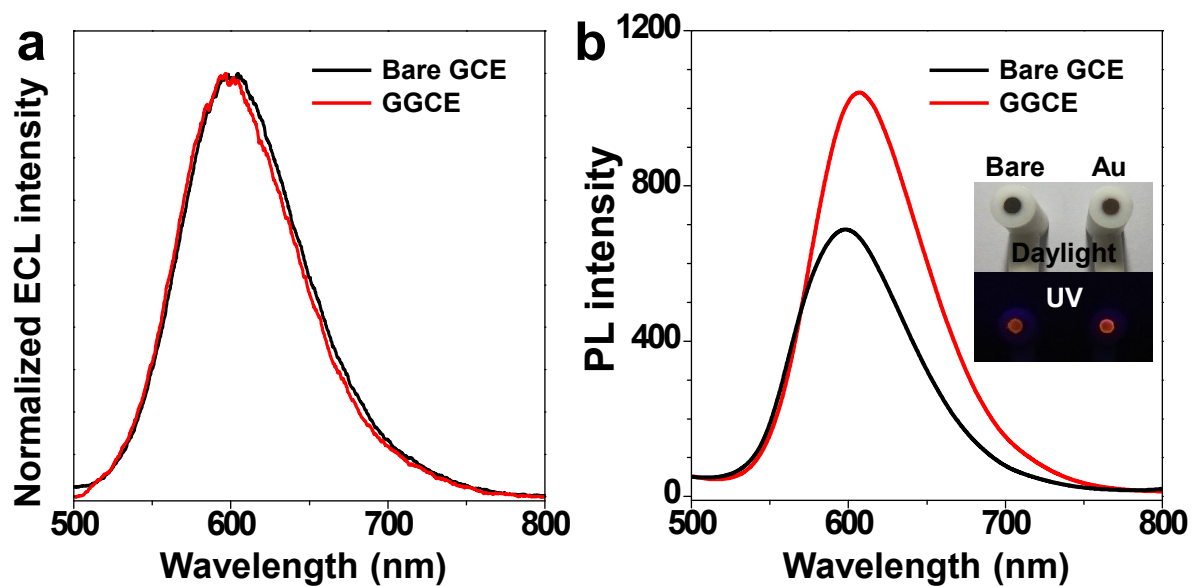


Figure S6. (a) Normalized ECL and (b) PL spectra of the AIEgen film on bare GCE and GGCE at 20 deposited cycles. Inset: digital photos under daylight and UV illumination (365 nm).

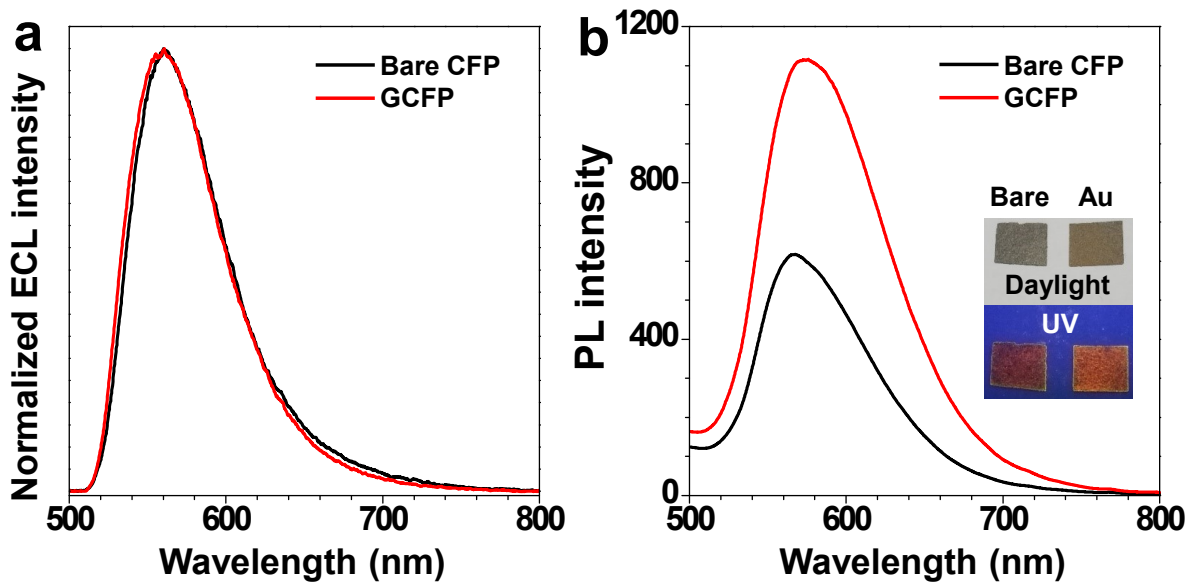


Figure S7. (a) Normalized ECL and (b) PL spectra of the AIEgen film on bare CFP and GCFP at 20 deposited cycles. Inset: digital photos under daylight and UV illumination (365 nm).

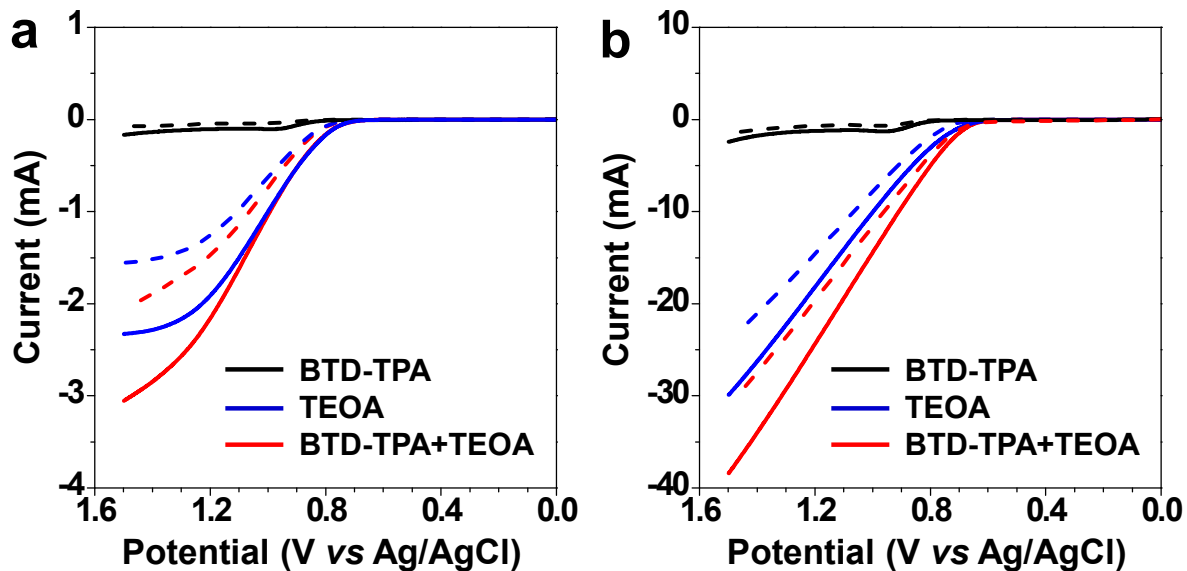


Figure S8. LSVs of the AIEgen film (156 ng/mm²), TEOA (300 mM), and their mixture using (a) bare GCE (dot line) and GGCE (20 cycles, solid line) and (b) bare CFP (dot line) and GCFP (100 cycles, solid line).

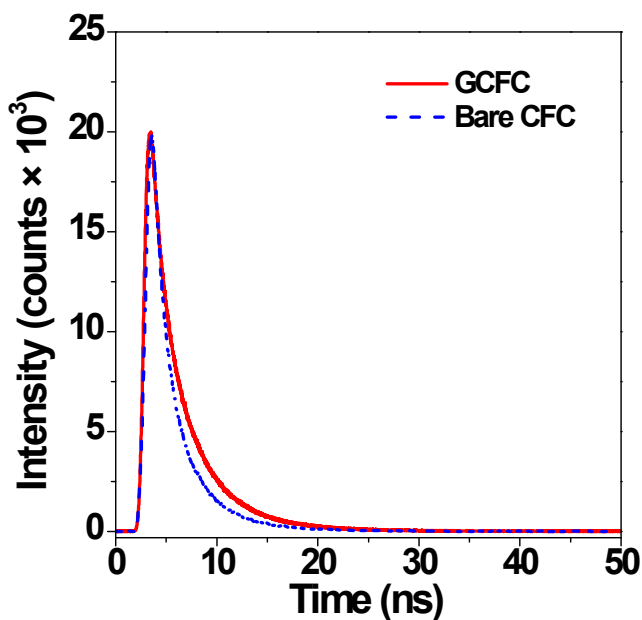


Figure S9. Time-resolved photoluminescence spectra of the AIEgen film on GCFC (20 deposition cycles) and bare CFC.

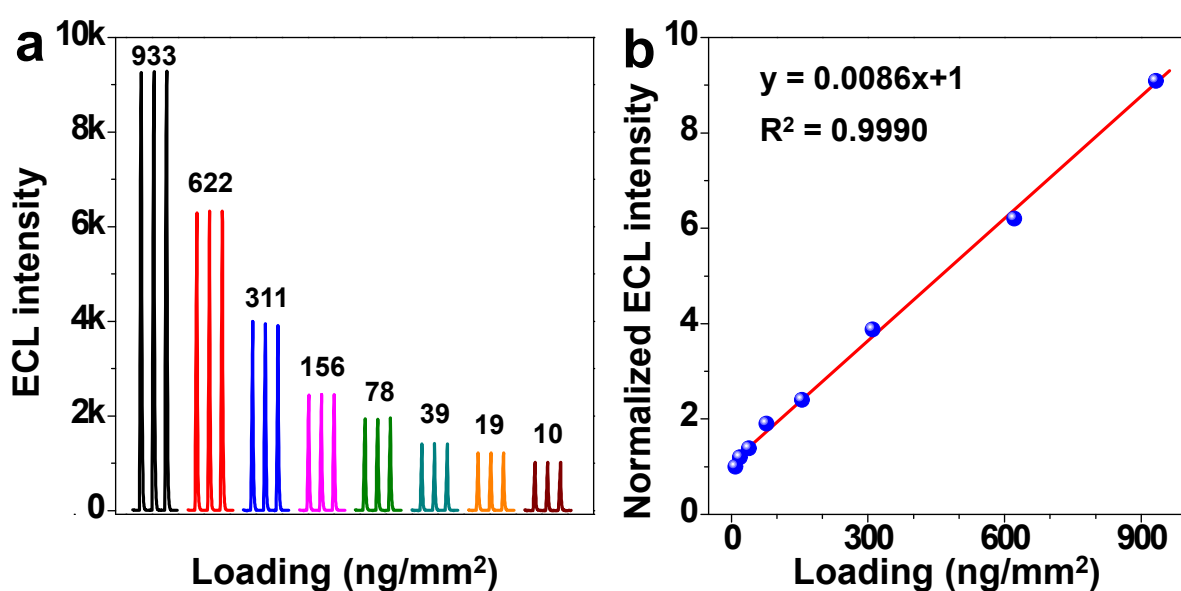


Figure S10. ECL intensity of the AIEgen film at various loadings on GCFC (20 deposition cycles).

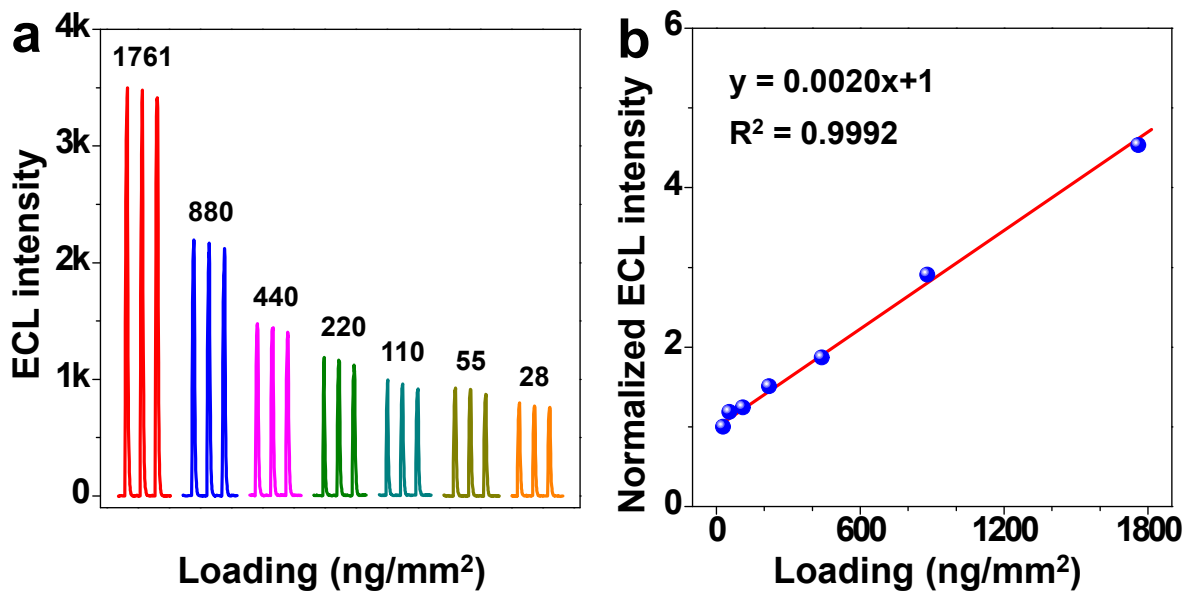


Figure S11. ECL intensity of the AIEgen film at various loadings on GGCE (20 deposition cycles).

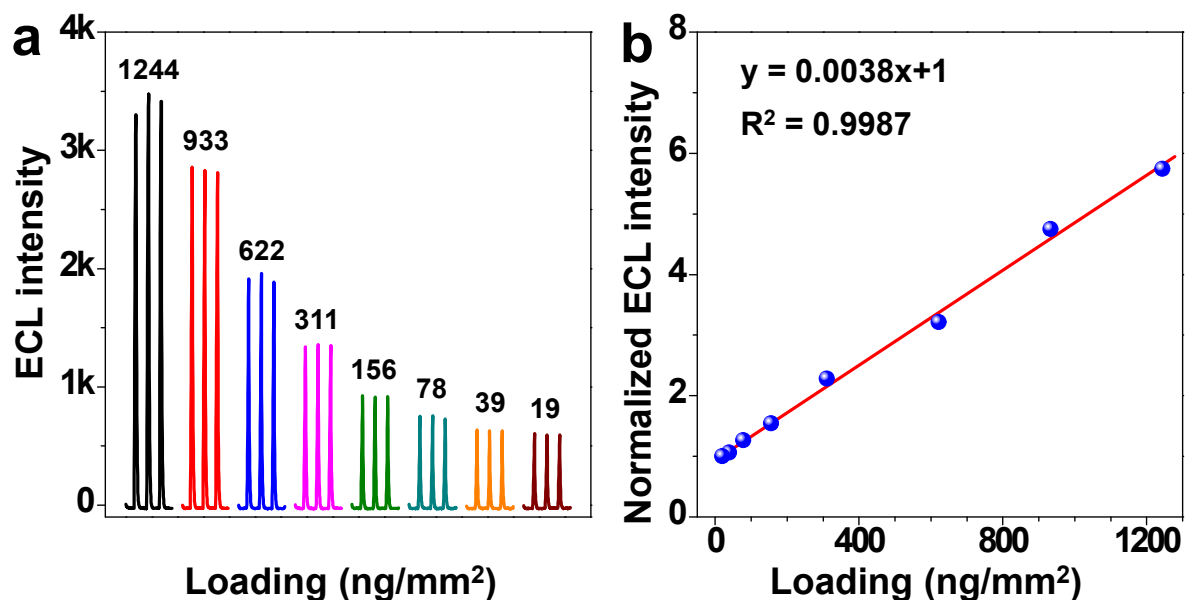


Figure S12. ECL intensity of the AIEgen film at various loadings on GCFP (100 deposition cycles).

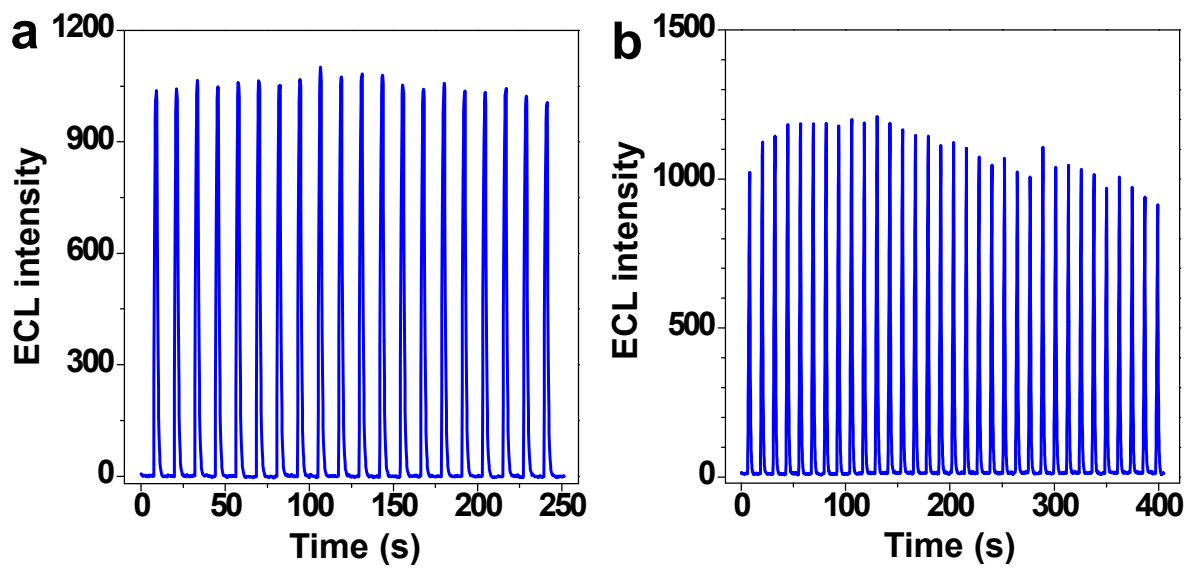


Figure S13. ECL stability of the AIEgen film on (a) GCFP (100 deposition cycles) and (b) GGCE (20 deposition cycles).

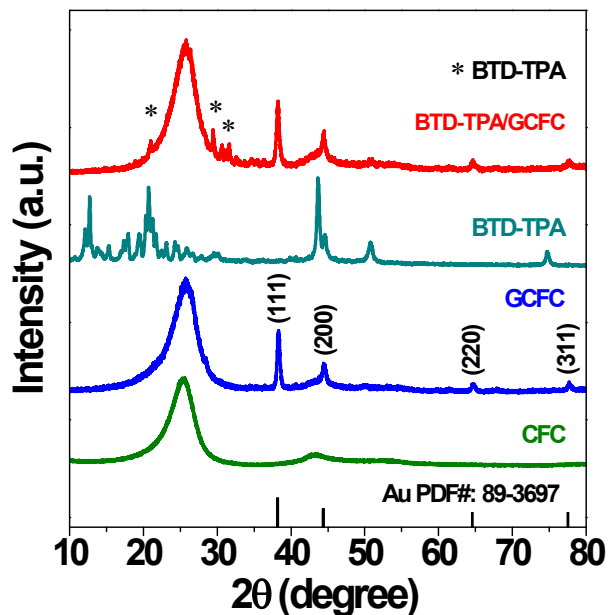


Figure S14. XRD patterns of CFC, GCFC, the AIEgen (BTD-TPA), and the AIEgen film on GCFC.

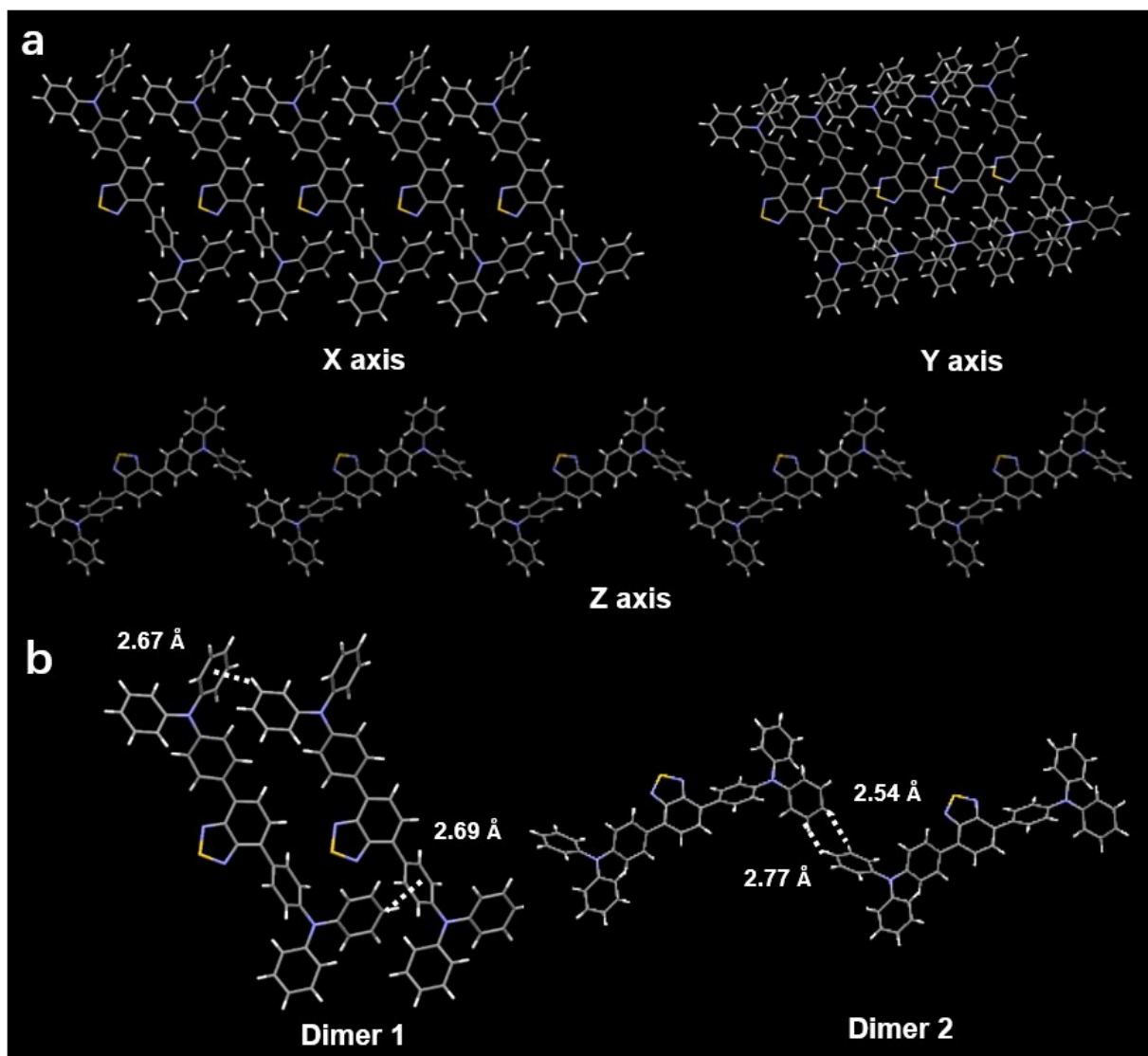


Figure S15. Crystal structures of the AIEgen (BTD-TPA). (a) View along X, Y, and Z axes, respectively. (b) Interaction between adjacent molecules.

Table S1 Comparison of the present research with other reported ECL sensors for detection of DA.

| Luminogens/Electrodes | Linear range | LOD | Reference |
|---|---|--|------------------|
| | (M) | (M) | |
| MIECLS/GCE ^[a] | 1.0×10^{-14} - 1.0×10^{-6} | 2.0×10^{-15} | 1 |
| ZnSe/GO@MWNTs/Ru(bpy) ₃ ²⁺ ^[b] | 1.0×10^{-9} - 1.0×10^{-5} | 6.0×10^{-8} | 2 |
| Au-WS ₂ /GE ^[c] | 5.0×10^{-9} - 2.0×10^{-4} | 3.23×10^{-9} | 3 |
| Pd NCs/GCE ^[d] | 1.0×10^{-12} - 1.0×10^{-8} | 4.6×10^{-13} | 4 |
| WO _x QDs/GCE ^[e] | 1.0×10^{-15} - 1.0×10^{-5} | 1.0×10^{-15} | 5 |
| TBPE-CMPs/GCE ^[f] | 1.0×10^{-9} - 1.0×10^{-3} | 8.5×10^{-10} | 6 |
| Eu ³⁺ -Cu NCs/GCE ^[g] | 1.0×10^{-11} - 5.0×10^{-4} | 1.0×10^{-11} | 7 |
| Luminol-DO/ITO ^[h] | 1.0×10^{-12} - 1.0×10^{-10} | 1.0×10^{-10} | 8 |
| Ru(bpy) ₃ ²⁺ /ITO | 2.5×10^{-7} - 2.0×10^{-5} | 2.28×10^{-7} | 9 |
| Luminol-DO/GCE | 1.0×10^{-12} - 1.0×10^{-8} | 5.2×10^{-12} | 10 |
| C545T MRs/GCE ^[i] | 2.0×10^{-8} - 4.0×10^{-6} | 5.19×10^{-9} | 11 |
| TPB NCs/GCE ^[j] | 5.0×10^{-9} - 1.0×10^{-5} | 3.1×10^{-9} | 12 |
| PEDOT-hosted Ag NCs/GCE ^[k] | 1.0×10^{-9} - 1.0×10^{-2} | 1.7×10^{-10} | 13 |
| Ru(bpy) ₃ ²⁺ /CNQD/GCE ^[l] | 1.0×10^{-6} - 1.0×10^{-3} | 5.0×10^{-7} | 14 |
| AIEgen film/GCFC | 1.0×10^{-15} - 1.0×10^{-6} | 3.16×10^{-16} | This work |

^[a]MIECLS: A quenching-type electrochemiluminescence sensor consist of upconversion nanoparticles, COFs-based ECL enhancement material and oligoaniline-crosslinked gold nanoparticles imprinting recognition sites. ^[b]ZnSe/GO@MWNTs/Ru(bpy)₃²⁺: ZnSe quantum dots/graphene oxide@multiwalled carbon nanotubes/Ru(bpy)₃²⁺. ^[c]Au-WS₂/GE: Au nanoparticles-WS₂ nanosheets/gold electrode. ^[d]Pd NCs: Pd nanocones. ^[e]WO_x QDs: tungsten oxide quantum dots. ^[f]TBPE-CMPs: 1,1,2,2-tetrakis(4-bromophenyl)ethane (TBPE)-based conjugated microporous polymers. ^[g]Eu³⁺-Cu NCs: Europium(III)-doped copper nanoclusters. ^[h]Luminol-DO: Luminol-Dissolved Oxygen. ^[i]C545T MRs: organic microrods of 2,3,6,7-tetrahydro-1,1,7,7,-tetramethyl-1H,5H,11H-10-(2-benzothiazolyl)quinolizino-[9,9a,1gh] coumarin. ^[j]TPB NCs: tetraphenyl-1,3-butadiene nanocrystals. ^[k]PEDOT-hosted Ag NCs: poly(3,4-ethylenedioxythiophene)-hosted Ag nanoclusters. ^[l]CNQD: carbon nitride quantum dots.

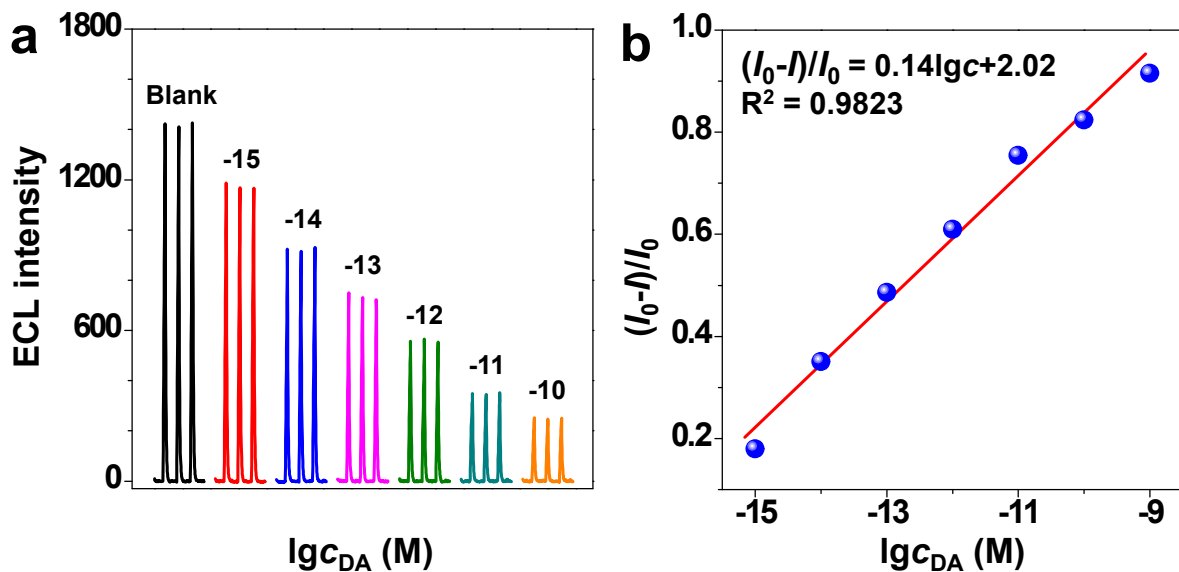


Figure S16. (a) ECL intensities of the AIEgen film (loading: 39 ng/mm²) on GCFC (20 deposition cycles) in the presence of various concentrations of DA. (b) Plot of $(I_0 - I)/I_0$ value against the logarithm of DA concentrations.

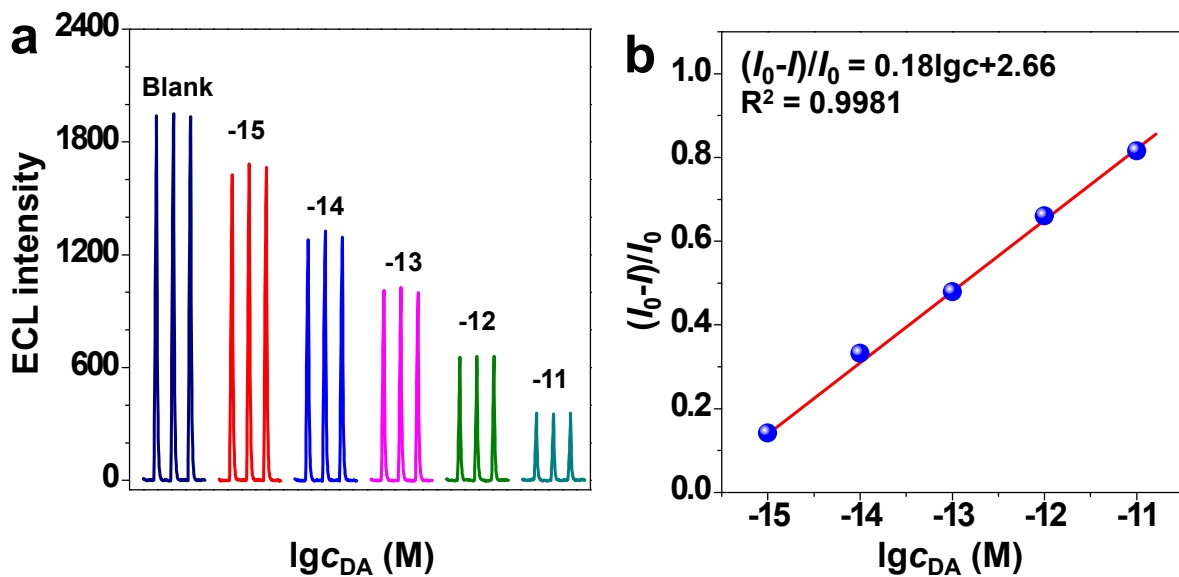


Figure S17. (a) ECL intensities of the AIEgen film (loading: 78 ng/mm²) on GCFC (20 deposition cycles) in the presence of various concentrations of DA. (b) Plot of $(I_0 - I)/I_0$ value against the logarithm of DA concentrations.

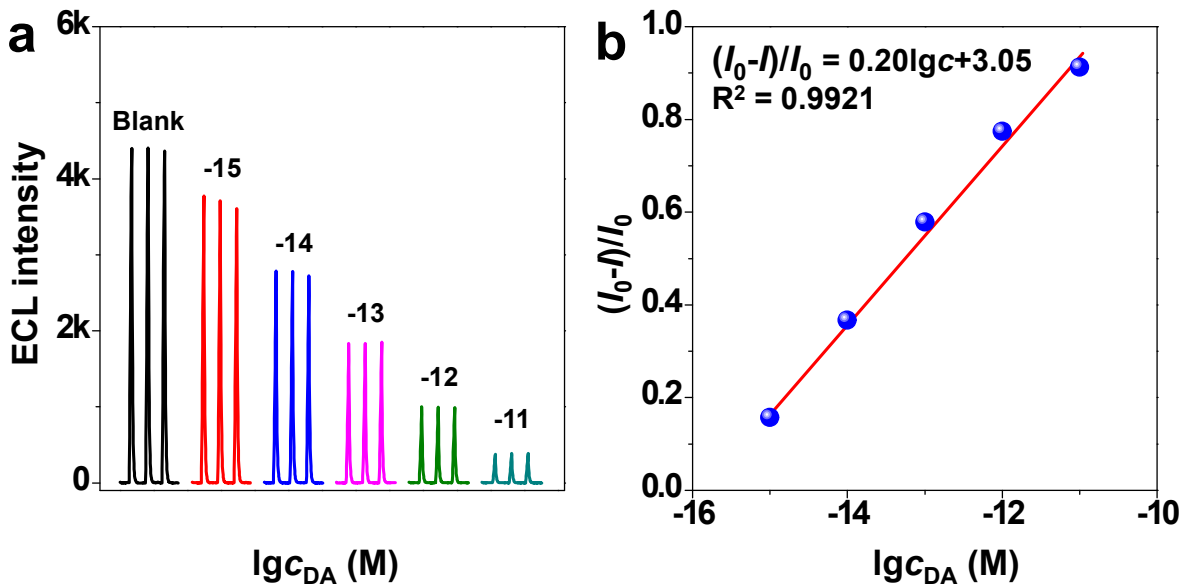


Figure S18. (a) ECL intensities of the AIEgen film (loading: 311 ng/mm²) on GCFC (20 deposition cycles) in the presence of various concentrations of DA. (b) Plot of $(I_0 - I)/I_0$ value against the logarithm of DA concentrations.

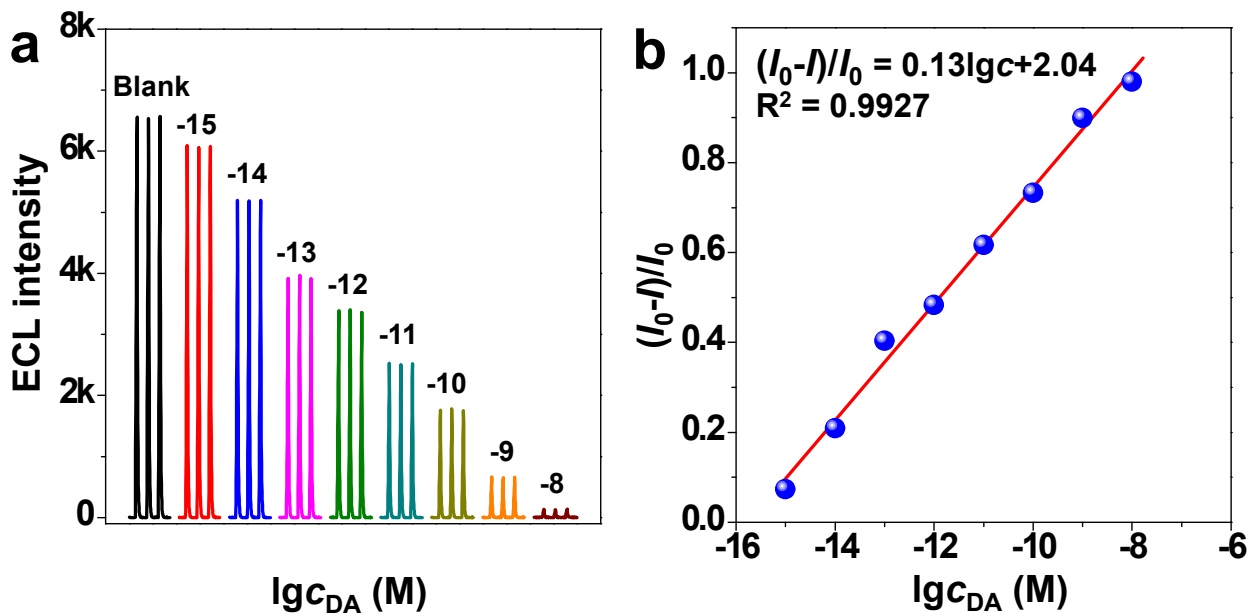


Figure S19. (a) ECL intensities of the AIEgen film (loading: 622 ng/mm²) on GCFC (20 deposition cycles) in the presence of various concentrations of DA. (b) Plot of $(I_0 - I)/I_0$ value against the logarithm of DA concentrations.

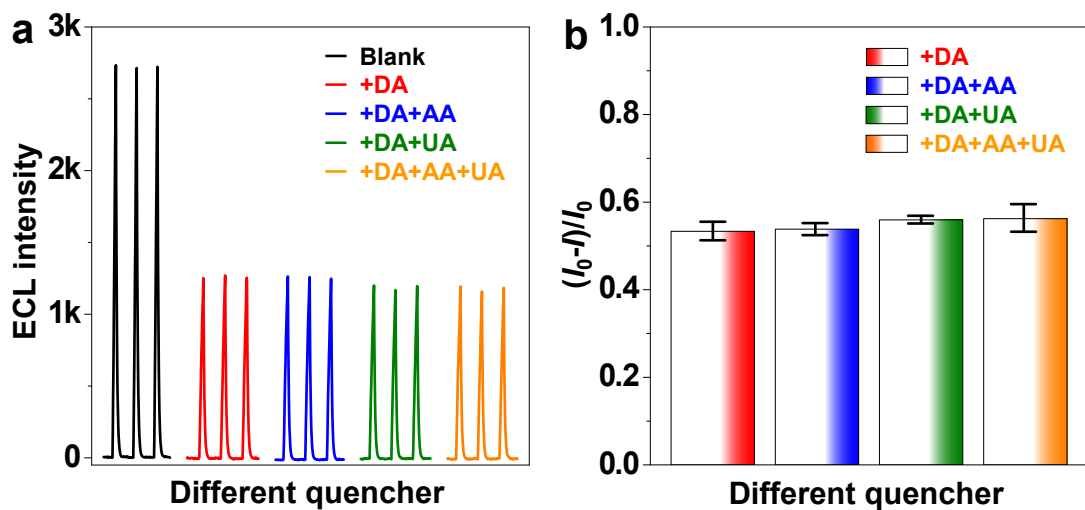


Figure S20. (a) ECL intensity and (b) $(I_0 - I)/I_0$ value of the AIEgen film in the presence of 1×10^{-11} M DA containing 100-fold concentrations of AA, UA, or a mixture of AA and UA.

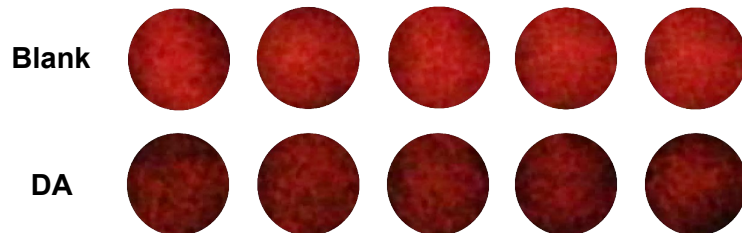
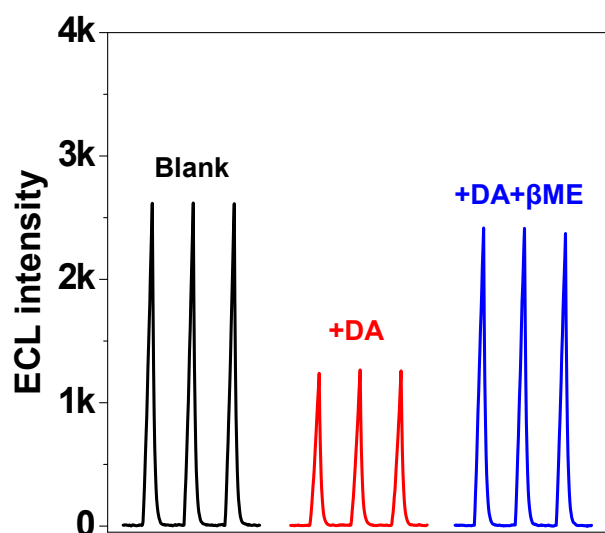


Figure S21. ECL images of the AIEgen film (loading: 156 ng/mm²) on GCFC (20 deposition cycles) in the absence and presence of DA (10^{-13} M).

Table S2 Grayscale analysis data of the AIEgen film on GCFC.

| $\lg c_{\text{DA}}$ ($\times 10^{-13} \text{ M}$) | Grayscale | Average value | $(G_0 - G)/G_0$ | c_{DA} ($\times 10^{-13} \text{ M}$) | Relative error (%) |
|--|---------------------------------|------------------|-----------------|--|-----------------------|
| 0 | 24.0, 23.2, 22.9, 21.6, 21.5 | 22.6 ± 1.08 | 0.40 ± 0.03 | 0.95 ± 0.50 | 5 |
| 1 | 15.1, 14.4, 13.2, 12.8, 12.2 | 13.6 ± 1.02 | | | |

**Figure S22.** ECL intensity of the AIEgen film/TEOA system (black line), with $1 \times 10^{-11} \text{ M}$ of DA (red line), with $1 \times 10^{-11} \text{ M}$ of DA and $2 \times 10^{-10} \text{ M}$ of 2-mercapoethanol (βME) (blue line), respectively.

References

- (1) Gu, Y.; Wang, J.; Shi, H.; Pan, M.; Liu, B.; Fang, G.; Wang, S. Electrochemiluminescence sensor based on upconversion nanoparticles and oligoaniline-crosslinked gold nanoparticles imprinting recognition sites for the determination of dopamine. *Biosens. Bioelectron.* **2019**, *128*, 129-136.
- (2) Tian, L.; Wang, X.; Wu, K.; Hu, Y.; Wang, Y.; Lu, J. Ultrasensitive electrochemiluminescence biosensor for dopamine based on ZnSe, graphene oxide@multi walled carbon nanotube and Ru(bpy)₃²⁺. *Sensor Actuat. B-Chem.* **2019**, *286*, 266-271.
- (3) Wang, Z.; Wang, X.; Zhu, X.; Lv, J.; Zhang, J.; Zhu, Q.; Dai, Z. Fabrication of non-destructive and enhanced electrochemiluminescence interface for reusable detection of cell-released dopamine. *Sensor Actuat. B-Chem.* **2019**, *285*, 438-444.
- (4) Wang, H. M.; Wang, C. C.; Wang, A. J.; Zhang, L.; Luo, X.; Yuan, P. X.; Feng, J. J. Green synthesis of Pd nanocones as a novel and effective electrochemiluminescence illuminant for highly sensitive detection of dopamine. *Sensor Actuat. B-Chem.* **2019**, *281*, 588-594.
- (5) Peng, H.; Liu, P.; Wu, W.; Chen, W.; Meng, X.; Lin, X.; Liu, A. Facile electrochemiluminescence sensing platform based on water-soluble tungsten oxide quantum dots for ultrasensitive detection of dopamine released by cells. *Anal. Chim. Acta* **2019**, *1065*, 21-28.
- (6) Cui, L.; Yu, S.; Gao, W.; Zhang, X.; Deng, S.; Zhang, C.-y. Tetraphenylenthene-Based Conjugated Microporous Polymer for Aggregation-Induced Electrochemiluminescence. *ACS Appl. Mater. Interfaces* **2020**, *12*, 7966-7973.
- (7) Zhuang, X.; Gao, X.; Tian, C.; Cui, D.; Luan, F.; Wang, Z.; Xiong, Y.; Chen, L. Synthesis of europium(iii)-doped copper nanoclusters for electrochemiluminescence bioanalysis. *Chem. Commun.* **2020**, *56*, 5755-5758.
- (8) Bushira, F. A.; Kitte, S. A.; Xu, C.; Li, H.; Zheng, L.; Wang, P.; Jin, Y. Two-Dimensional-Plasmon-Boosted Iron Single-Atom Electrochemiluminescence for the Ultrasensitive Detection of Dopamine, Hemin, and Mercury. *Anal. Chem.* **2021**, *93*, 9949-9957.

- (9) Ding, H.; Guo, W.; Zhou, P.; Su, B. Nanocage-confined electrochemiluminescence for the detection of dopamine released from living cells. *Chem. Commun.* **2020**, *56*, 8249-8252.
- (10) Bushira, F. A.; Wang, P.; Jin, Y. High-Entropy Oxide for Highly Efficient Luminol-Dissolved Oxygen Electrochemiluminescence and Biosensing Applications. *Anal. Chem.* **2022**, *94*, 2958-2965.
- (11) Yan, M.; Xin, J.; Fan, L.; Ye, J.; Xiao, T.; Huang, J.; Yang, X. Electrochemistry and Electrochemiluminescence of Coumarin Derivative Microrods: Mechanism Insights. *Anal. Chem.* **2021**, *93*, 3461-3469.
- (12) Liu, J.-L.; Zhang, J.-Q.; Zhou, Y.; Xiao, D.-R.; Zhuo, Y.; Chai, Y.-Q.; Yuan, R. Crystallization-Induced Enhanced Electrochemiluminescence from Tetraphenyl Alkene Nanocrystals for Ultrasensitive Sensing. *Anal. Chem.* **2021**, *93*, 10890-10897.
- (13) Nie, Y.; Tao, X.; Zhou, Y.; Yuan, X.; Zhuo, Y.; Chai, Y.-q.; Yuan, R. Kill Three Birds with One Stone: Poly(3,4-ethylenedioxythiophene)-Hosted Ag Nanoclusters with Boosted Cathodic Electrochemiluminescence for Biosensing Application. *Anal. Chem.* **2021**, *93*, 1120-1125.
- (14) Qin, Y.; Wang, Z.; Xu, J.; Han, F.; Zhao, X.; Han, D.; Liu, Y.; Kang, Z.; Niu, L. Carbon Nitride Quantum Dots Enhancing the Anodic Electrochemiluminescence of Ruthenium(II) Tris(2,2'-bipyridyl) via Inhibiting the Oxygen Evolution Reaction. *Anal. Chem.* **2020**, *92*, 15352-15360.